Fluorescence Imaging of Two-Photon Linear Dichroism: Cholesterol Depletion Disrupts Molecular Orientation in Cell Membranes

Richard K. P. Benninger,* Björn Önfelt,*† Mark A. A. Neil,* Daniel M. Davis,† and Paul M. W. French*
*Department of Physics and †Department of Biological Sciences, Imperial College London, London SW7 2AZ, United Kingdom

ABSTRACT The plasma membrane of cells is an ordered environment, giving rise to anisotropic orientation and restricted motion of molecules and proteins residing in the membrane. At the same time as being an organized matrix of defined structure, the cell membrane is heterogeneous and dynamic. Here we present a method where we use fluorescence imaging of linear dichroism to measure the orientation of molecules relative to the cell membrane. By detecting linear dichroism as well as fluorescence anisotropy, the orientation parameters are separated from dynamic properties such as rotational diffusion and homo energy transfer (energy migration). The sensitivity of the technique is enhanced by using two-photon excitation for higher photo-selection compared to single photon excitation. We show here that we can accurately image lipid organization in whole cell membranes and in delicate structures such as membrane nanotubes connecting two cells. The speed of our wide-field imaging system makes it possible to image changes in orientation and anisotropy occurring on a subsecond timescale. This is demonstrated by time-lapse studies showing that cholesterol depletion rapidly disrupts the orientation of a fluorophore located within the hydrophobic region of the cell membrane but not of a surface bound probe. This is consistent with cholesterol having an important role in stabilizing and ordering the lipid tails within the plasma membrane.

INTRODUCTION

Many protein-protein interactions, crucial for biological function, take place in the plasma membrane of the cell or at the intercellular contact between two cells, e.g., at the immunological synapse (Davis, 2002). These interactions are dependent on the local lipid environment, which affects properties such as partition of proteins into different domains (Harder et al., 1998; Eleme et al., 2004), rate of lateral diffusion in the membrane (Pralle et al., 2000) or hopping between transient confinement zones (Dietrich et al., 2002; Kusumi et al., 2004). Recently the role of membrane heterogeneity in cell function has received intense scrutiny. Some functional properties have suggested the existence of 'lipid rafts', which are microdomains rich in sphingolipids and cholesterol (Simons and Ikonen, 1997; Edidin, 2003; Simons and Vaz, 2004). However, it has proven difficult to study these domains in living cells; biochemical methods, involving isolation of detergent resistant membrane, are quite invasive and dependent on the detergents used (Schuck et al., 2003). Imaging methods, which often involve clustering of domains using antibodies or cholera toxin B subunit that binds the raft marker lipid GM1, have not unequivocally proven the existence of rafts. Methods to noninvasively study lipid heterogeneity and correlate a change in lipid environment with function in live cells, are sorely needed (Munro, 2003). The lipid probe Laurdan gives one interesting example of how a change in lipid environment can be probed by looking at the spectral shift caused by presence of water in the membrane (Gaus et al., 2003).

Another property that is fundamental for membrane-protein function is the orientation of the protein relative to the membrane (Doucey et al., 2004; Mitra et al., 2004). Several studies of anisotropy of molecules in macroscopically oriented lipid environments have been reported, including studies of: 1), Lipid bilayers or Langmuir-Blodgett films that are mounted at an angle from the incoming beam allowing measurements of both absorbance and fluorescence (Karolin et al., 1994; Edmiston et al., 1996; Tronin et al., 2000; Lopes and Castanho 2004); 2), Polarized fluorescence imaging of vesicles or cell membranes (Axelrod 1979; Blackman et al., 1996; Sund et al., 1999; Rocheleau et al., 2003); 3), Linear dichroism (LD) of vesicles that are deformed in a laminar flow creating an experimental orientation axis (Ardhammar et al., 1998; Brattwall et al., 2003); and 4), The effect of refractive index on radiative decay rate of probes orientated in lipid vesicles (Toptygin and Brand 1993; Krishna and Periasamy 1998).

In this article, we present a method, based on fluorescence-detected LD (or absorption anisotropy) to study orientation of fluorescent probes bound to the plasma membranes of living cells (the probes used are shown in Fig. 1). The benefit of imaging fluorescence-detected LD is that it reports the steady-state orientation of a probe with minimal contamination of the signal from depolarizing effects, such as transfer of energy between probes (energy migration or homo FRET) or rotational diffusion of the probe. The two latter properties are of a dynamic nature and in many ways are more interesting for function than the steady state orientation. We

Submitted July 24, 2004, and accepted for publication October 19, 2004.

Richard K. P. Benninger and Björn Önfelt contributed equally to this work.
Daniel M. Davis and Paul M. W. French contributed equally to this work.
Address reprint requests to Björn Önfelt, Tel.: 44-20-7594-5474; Fax: 44-20-7594-3044 Email: b.onfelt@imperial.ac.uk.

0006-3495/05/01/609/14 $2.00
doi: 10.1529/biophysj.104.050096

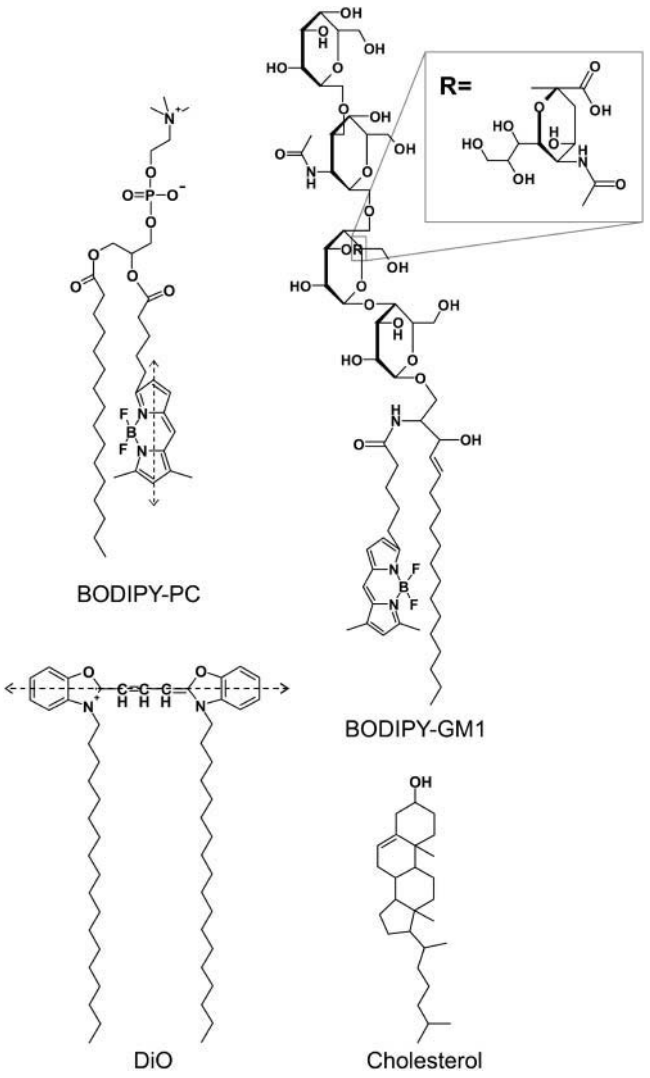

FIGURE 1 Structures of the lipid probes used in this study. Dashed arrows denote the direction of the two-photon absorption transition moments at 920 nm for BODIPY and DiO, respectively.

believe it may be attractive to use LD to determine the average probe orientation and thereafter to study the dynamic properties by fluorescence anisotropy (r). In this article, however, we focus on determining the orientation parameters using LD.

Our LD experiments were performed using a high-speed multiphoton microscope that utilizes multiple excitation foci such that the sample can be scanned rapidly and imaged onto a wide-field detector at frame rates exceeding video rate. This approach allows us to use the full available power from the laser source, and we achieve the high signal to noise ratio required for ratiometric imaging without significant photo-bleaching. The high acquisition speed makes it possible to correlate spatial and temporal changes in lipid environment with cell function. To demonstrate this we carry out time-lapse studies of how cholesterol depletion by methyl-β-cyclodextrin (MβCD) affects the order of a surface bound fluorescent probe (DiO) and a fluorescent probe embedded within the membrane (BODIPY-PC) (see structures in Fig. 1).

THEORY

Linear dichroism

Linear dichroism is defined as

$$LD = A_{\parallel} - A_{\perp}, \tag{1}$$

where $A_{\parallel}$ and $A_{\perp}$ are the absorption of light polarized parallel and perpendicular to a defined experimental axis, respectively. More useful for determining orientation is the reduced linear dichroism (LD^{r}), which is the LD^{r} normalized to the isotropic absorbance. Here we use the fluorescence signal to calculate the LD and, in doing so, we assume that the calculated isotropic fluorescence signal is proportional to the absorbance according to Eqs. 2, a and b,

$$A_{\parallel} \approx c_1(I_{ZZ} + 2I_{ZY}) \tag{2a}$$

$$A_{\perp} \approx c_2(I_{YY} + 2I_{YZ}), \tag{2b}$$

where I is the fluorescence intensity detected collinear to the excitation for a given combination of excitation and emission polarizations (Z and Y), respectively. The vectors Z and Y lie in the plane of the image, orthogonal to each other and to the optical axis. c_1 and c_2 are constants of proportionality. For an oriented sample, this way of calculating the total fluorescence is strictly only accurate when the sample has uniaxial orientation symmetry and the excitation polarization is parallel with the axis of symmetry. The error introduced by the deviation from this condition around the cell circumference, however, is always a relatively small ($<5\%$) and we have neglected it in the subsequent analysis. A more detailed analysis of this error can be found in the supplemental material. The formula for the reduced linear dichroism is

$$LD^{\mathrm{r}} = \frac{A_{\parallel} - A_{\perp}}{A_{\parallel} + 2A_{\perp}} \approx \frac{c_1(I_{ZZ} + 2I_{ZY}) - c_2(I_{YY} + 2I_{YZ})}{c_1(I_{ZZ} + 2I_{ZY}) + 2c_2(I_{YY} + 2I_{YZ})}. \tag{3}$$

LD^{r} can be used either to determine how a transition moment is directed in a molecule or how a molecule is oriented relative to an orientation axis. In this study we aim to investigate molecular orientation utilizing fluorophores where the direction of the transition moments are known in the molecular frame. To get a nonzero LD^{r} value the absorbing molecule has to be macroscopically orientated relative to the experimental axis. Such orientation can, for example, be achieved for chromophores in membrane environments as described in the introduction, bound to actin fibers in muscle structures (Xiao et al., 1996; Borejdo et al., 2004), in stretched polymer films (Thulstrup and Michl, 1982) or bound to flow-oriented DNA (Nordén et al., 1992).

In this study we use the plane of a sectioned image to assess the experimental orientation axis as being directed normal to the edges of the round cell. Although the image directly allows determination of this experimental orientation axis, the plasma membrane of a living cell also has another macroscopic orientation axis, which is determined by the topology of the cell membrane, i.e., membrane ruffling. In many cases, this topology is too small to resolve in an optical microscope due to the diffraction limited resolution ($\lambda/2$). Microscopically, lipids in the cell membrane are assembled in an ordered way; the polar headgroups are directed toward either of the surfaces of the bilayer while the lipid tails are pointing inwards. This ordered matrix will constrain molecules or proteins to orientate in a specific way. Some fluorophores are embedded within the hydrophobic region of the membrane, in which case its microscopic orientation is determined by its interaction with acyl chains of surrounding lipids or for example cholesterol (Ohvo-Rekila et al., 2002), whereas other probes have the chromophore on the surface of the lipid layer, in which case interactions with the polar head groups may be more important to determine its microscopic orientation. Thus, our measured linear dichroism can be divided into two parts, one related to the macroscopic orientation (membrane topology) and one that has to do with the microscopic orientation (molecular orientation in the bilayer). This is a complication when studying orientation in membranes of live cells since it is not straightforward to disentangle the contributions from each of these factors. In our initial theoretical approach presented here, we do not attempt to separate the two contributions but combine them into a 'mean tilt' and treat the membrane in an equatorial plane of the cell as circular.

Imaging two-photon LD of chromophores orientated in a circular membrane

A method for studying orientation and dynamics of fluorophores in membrane has been outlined by Van der Meer et al. (1982) and applied to circular membrane systems (Blackman et al., 1996; Rocheleau et al., 2003). In those studies, they used a model of the orientation and the depolarizing process to gain an understanding of the dynamics of the fluorophore under question. In this study, however, we are looking at just the steady state orientation using a method where the depolarizing process (rotational diffusion, energy transfer) as well as the angle between absorption and emission transition moments have minimal contribution to the measured LD^{r}.

In this section we use a vectorial approach to derive a model that gives the LD^{r} as a function of angle (α) around the cell for a given probe orientation. We have chosen to look at two different types of lipid probes where the chromophores have distinct orientations in the membrane. For DiO the chromophore is located in the head group and the absorption transition moment can be assumed directed along the long-axis of the chromophore as indicated by the gray arrows in Figs. 1 and 2 (Castanho et al., 2003). To be more precise, the DiO chromophore has two absorption transition moments of similar magnitude orientated symmetrically around the long axis of the chromophore, resulting in a small component perpendicular to the long axis also at high wavelengths. However, this component is of very low magnitude (Sund et al., 1999), justifying our approximated transition moment direction.

For further analysis, we define the molecular orientation axis, common for the three investigated probes, as being directed along the acyl chains of the lipid probes. Thus, the transition moment of DiO is assumed to be orientated perpendicular to this molecular orientation axis and the transition moment of the BODIPY probes are assumed to orient close to parallel with the molecular orientation axis. The molecular orientation axis is defined since the general structure of the lipid probes dictates the orientation of the chromophores in the membrane, but it is important to point out that the conformation of the molecules may vary and the only thing we can measure are the orientations of the absorption transition moments.

If the DiO molecule orientates perfectly in the membrane, such that the molecular orientation axis is parallel with that of the membrane normal, the absorption transition moment of the chromophore is orientated parallel with the membrane surface. Assuming that there is no preferred orientation of the DiO molecule around the molecular orientation axis (uniaxial orientation) the transition moment orientation with respect to the membrane normal is

$$\vec{\boldsymbol{\mu}}'_{\mathrm{DiO}} = \begin{bmatrix} |\mu|\sin\eta \\ |\mu|\cos\eta \\ 0 \end{bmatrix}, \tag{4a}$$

where η is a rotation around the molecular orientation axis as shown in Fig. 2 *a*. The other probes we look at have the chromophore BODIPY located on the end of one of the lipid tails, with the transition moment orientated along the long-axis of the chromophore as indicated by the gray arrow in Fig. 1 (Karolin et al., 1994). Fig. 1 depicts the long axis of BODIPY orientated parallel with the molecular orientation axis, which may not be the preferred conformation. However, if the BODIPY probes orientate in the membrane such that the chromophore long-axis is parallel to the membrane normal, then the transition moment orientation with respect to the membrane normal is

$$\vec{\boldsymbol{\mu}}'_{\mathrm{BODIPY}} = \begin{bmatrix} 0 \\ 0 \\ |\mu| \end{bmatrix} \tag{4b}$$

and thus independent of orientation around the molecular orientation axis.

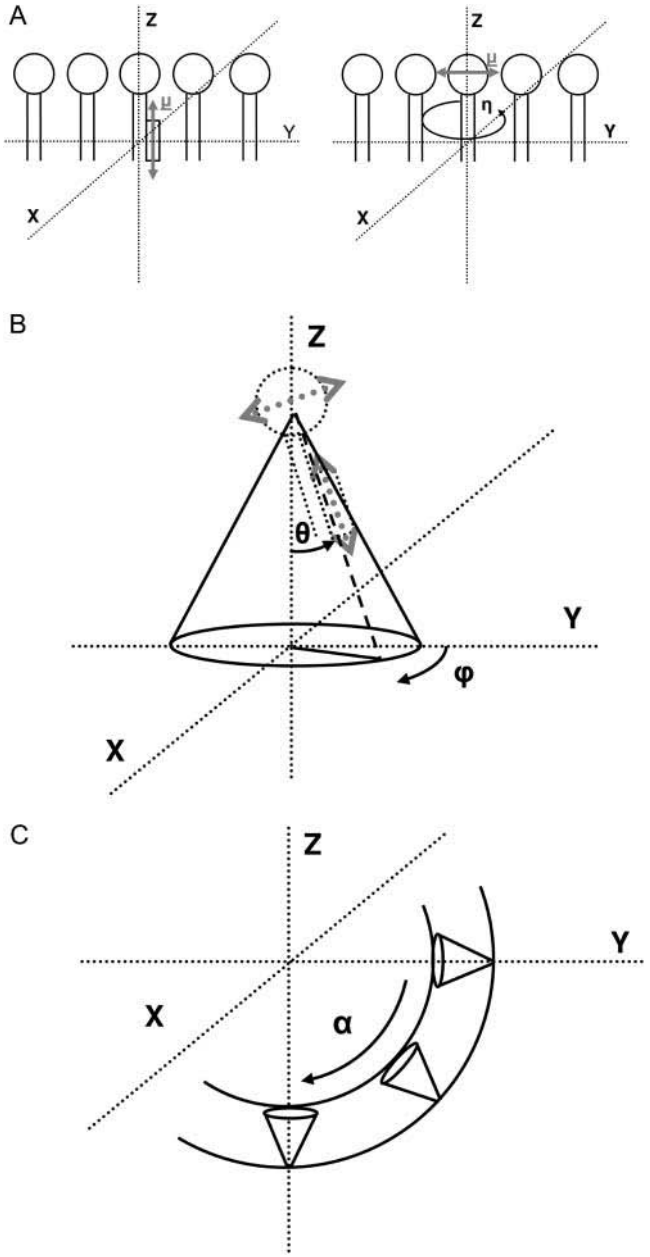

FIGURE 2 Definition of the axes and angles used to derive LD^{r} model. (*A*) Transition moment orientation for BODIPY (*left*) and DiO (*right*) when perfectly orientated in the membrane. The rotation indicated by η refers to uniaxial orientation in the *XY* plane. (*B*) Disorientation of the lipid probes to the membrane normal can be described by the angles θ and φ. (C) The angle α refers to the rotation around the plasma membrane at the equatorial section of the cell. Excitation polarizations are either along the laboratory *Z*-axis (parallel) or along the laboratory *Y*-axis (perpendicular).

These probes will not, however, orientate perfectly in the membrane due to the fluid nature of the lipid constituents. A tilt from the membrane normal, θ, and a rotation around the membrane normal, φ, will account for these deviations from perfect alignment of the transition moment.

$$\vec{\boldsymbol{\mu}}'' = \begin{bmatrix} \cos\varphi & \sin\varphi & 0 \\ -\sin\varphi & \cos\varphi & 0 \\ 0 & 0 & 1 \end{bmatrix} \begin{bmatrix} 1 & 0 & 0 \\ 0 & \cos\theta & -\sin\theta \\ 0 & \sin\theta & \cos\theta \end{bmatrix} \vec{\boldsymbol{\mu}}'. \quad (5)$$

For an ensemble of molecules, we can average over all φ since the membrane is assumed to have uniaxial symmetry, and about η if we assume that the chromophore has rotational symmetry about the molecular orientation axis (i.e., DiO). For the BODIPY, intramolecular interactions may affect rotational freedom of the chromophore. However, at this stage we simplify our model by not taking that into account. Below we discuss the effect of considering a distribution of chromophore orientations.

Two-photon imaging creates an optical section of the equatorial plane with a thickness of ~500 nm. In our analysis we neglect the membrane curvature normal to the image plane (Blackman et al., 1996) and only consider a rotation around the cell. Thus in the lab frame, the membrane normal and thus the transition moment relative to the membrane normal is transformed as below:

$$\vec{\boldsymbol{\mu}}''' = \begin{bmatrix} 1 & 0 & 0 \\ 0 & \cos\alpha & -\sin\alpha \\ 0 & \sin\alpha & \cos\alpha \end{bmatrix} \vec{\boldsymbol{\mu}}''. \quad (6)$$

Laser illumination is polarized parallel and perpendicular to the laboratory *Z*-axis, respectively:

$$\vec{\mathbf{E}}_{\parallel} = \begin{bmatrix} 0 \\ 0 \\ E \end{bmatrix} \quad \vec{\mathbf{E}}_{\perp} = \begin{bmatrix} 0 \\ E \\ 0 \end{bmatrix}. \quad (7)$$

Thus, parallel and perpendicular absorption for a single transition moment is

$$A_{\parallel} = |\vec{\boldsymbol{\mu}}''' \cdot \vec{\mathbf{E}}_{\parallel}|^2 \quad (8a)$$

$$A_{\perp} = |\vec{\boldsymbol{\mu}}''' \cdot \vec{\mathbf{E}}_{\perp}|^2. \quad (8b)$$

The resultant absorption is thus a function of ψ, the orientation of the absorption transition moment in the molecular frame of the chromophore (for DiO and BODIPY ψ is known); θ, the molecular orientation in the membrane (contaminated by membrane topology); and α, the image coordinate in the cell being examined:

$$\langle A_{\parallel}(\psi,\theta,\alpha)\rangle = \frac{1}{4\pi^2}\int d\eta \int d\varphi\, A_{\parallel}(\psi,\eta,\theta,\varphi,\alpha) \quad (9a)$$

$$\langle A_{\perp}(\psi,\theta,\alpha)\rangle = \frac{1}{4\pi^2}\int d\eta \int d\varphi\, A_{\perp}(\psi,\eta,\theta,\varphi,\alpha) \quad (9b)$$

And hence the *LD* as a function of α, for a given molecular orientation θ at transition moment orientation ψ is

$$LD^{r}(\psi,\theta,\alpha) = 3\,\frac{\langle A_{\parallel}(\psi,\theta,\alpha)\rangle - \langle A_{\perp}(\psi,\theta,\alpha)\rangle}{\langle A_{\parallel}(\psi,\theta,\alpha)\rangle + 2\langle A_{\perp}(\psi,\theta,\alpha)\rangle}, \quad (10)$$

which for $\alpha = 90$ and 270° reduces to the more general equation

$$LD^{r} = \frac{1}{2}(3\langle\cos^2\theta\rangle - 1)\frac{3}{2}(3\cos^2\psi - 1). \qquad (11)$$

This is the general case of measuring absorption or, as we do here, measuring total fluorescence emission to be proportional to absorption. In the case of two-photon microscopy, the chromophore absorbs two photons simultaneously in the IR, and emits a single photon in the visible. This means that the fluorescence emission is proportional to the absorption squared. This requires a modification of the LD^{r} formula by taking the square of the absorption (i.e., $|\mathbf{E}\cdot\mu|^4$) before integrating over η and φ:

$$\langle A_{\parallel}^{2p}(\psi,\theta,\alpha)\rangle = \frac{1}{4\pi^2}\int d\eta \int d\varphi\, |A_{\parallel}(\psi,\eta,\theta,\varphi,\alpha)|^2 \quad (12a)$$

$$\langle A_{\perp}^{2p}(\psi,\theta,\alpha)\rangle = \frac{1}{4\pi^2}\int d\eta \int d\varphi\, |A_{\perp}(\psi,\eta,\theta,\varphi,\alpha)|^2. \qquad (12b)$$

The integrals in Eqs. 12, a–b, can be analytically or numerically solved to form the LD^{r}.

Comparing single- versus two-photon LD

Fig. 3, *A* and *B*, shows the LD^{r} value of single- and two-photon excitation as a function of mean tilt. It is evident that for weakly orientated samples ($30° < \theta < 70°$), two-photon is more sensitive than single photon LD^{r}. This is however contrasted by the change in LD^{r} for highly orientated samples, where single photon is more sensitive. Fig. 3, *C* and *D*, show how the LD^{r} value is expected to change with angle, α, around the cell for probes of the two types we have described above (general direction of the absorption transition moment perpendicular or parallel to the cell surface) tilted at an angle θ.

Depolorization due to high numerical aperture excitation

Generally to achieve sufficient power density such that two-photon absorption occurs and to get high spatial resolution, the specimen has to be illuminated by ultra-short laser pulses through an objective with a high numerical aperture (NA). When using a high NA objective, the excitation polarization is not generally maintained at the focus, although this effect is less pronounced for multiphoton excitation, owing to the nonlinear excitation. Some of the light enters the focus at very high angles, so the polarization is tilted with respect to the polarization on the back aperture. This problem also occurs in the fluorescence emission (Axelrod, 1979), but when measuring the total intensity the effect of this cross talk is significantly reduced. Therefore we only consider the effect of high NA on excitation polarization.

To correct for the excitation polarization, we will work out the vector field at the focal plane for a linear input polarization. The *E* field at the focal plane given as

$$E_Z = -iA[I_0(u=0,v) + I_2(u=0,v)\cos(2\phi)] \qquad (13a)$$

$$E_Y = -iAI_2(u=0,v)\sin(2\phi) \qquad (13b)$$

$$E_X = -2AI_1(u=0,v)\cos(\phi), \qquad (13c)$$

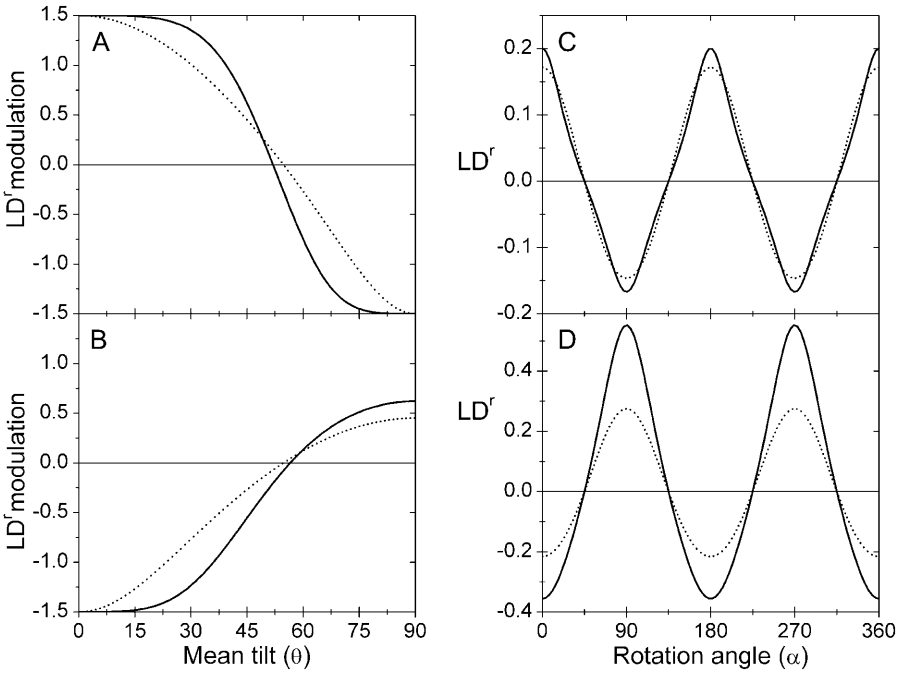

FIGURE 3 Comparison of one and two-photon excitation. LD^{r} modulation as a function of tilt with respect to membrane normal for an uniaxially oriented probe with the transition moment parallel (*A*, corresponding to BODIPY) and perpendicular (*B*, corresponding to DiO) to the molecular orientation axis. It can be seen that the two-photon absorption (*solid line*) is steeper for weakly orientated fluorophore (30–70° tilts) and therefore more sensitive. In contrast, for high orientations (0–30 and 70–90° tilts) one-photon excitation (*dotted line*) is more sensitive. LD^{r} profile for one- (*dotted line*) and two-photon (*solid line*) as a function of rotation angle around the cell for BODIPY with a fixed tilt of 48° (*C*) and DiO with a tilt of 38° (*D*). These tilt angles are typically measured for these probes in cell membranes. Note that in *C*, the shapes are different for one- and two-photon LD^{r}, respectively, but the modulation is roughly the same. In *D*, the modulation is much higher for two-photon absorption compare to one-photon.

where Z is the original excitation polarization direction, Y is the perpendicular polarization direction, and X is the optical axis. I_0, I_1, and I_2 are integrals formulated in Richards and Wolf (1959) and are functions of the NA and position in the coordinate system; u, v, and ϕ refer to optical units in cylindrical coordinates ($u = 0$ is the focal plane), and A is a constant to give the absolute electric field. We model the vector field after linearly polarized excitation using the above Eqs. 13, a–c, for the objective used in the experiments as well as considering that we are imaging into a watery sample. We thus neglect very high aperture rays and any aberrations due to refractive index mismatches, and use an NA of 1.2 into a media of refractive index 1.4. The above vector field is evaluated at the focus after excitation polarized along the Z (parallel) and Y (perpendicular) axis, and we form the absorption as a function of transition moment orientation. This absorption is integrated over the point spread function at the focal plane to give the following function for high NA two-photon absorption, where M_1 to M_6 are constants, with M_1 dominating in the low NA range:

$$A_{\parallel}^{2p} \propto M_1\mu_z^4 + M_2\mu_y^4 + M_3\mu_x^4 + M_4\mu_z^2\mu_x^2 + M_5\mu_z^2\mu_y^2 + M_6\mu_y^2\mu_x^2 \tag{14a}$$

$$A_{\perp}^{2p} \propto M_1\mu_y^4 + M_2\mu_z^4 + M_3\mu_x^4 + M_4\mu_y^2\mu_x^2 + M_5\mu_y^2\mu_z^2 + M_6\mu_z^2\mu_x^2. \tag{14b}$$

Constants M_1 to M_6 can be calculated and the corrected absorption can be evaluated and used in Eqs. 12, a and b.

MATERIALS AND METHODS

Cell lines, chemicals, and sample preparation

The Burkitt's lymphoma B cell line transfected to express β_2 microglobulin (DAUDI/class I+) has been described earlier (Cosman et al., 2001). Cells were cultured in RPMI medium (Invitrogen, Carlsbad, CA) containing heat inactivated fetal bovine serum (FBS) (10%), L-glutamine (2 nM) and penicillin-streptomycin (50 units/ml). Human embryonic kidney (HEK) 293T cells were cultured in DMEM (Invitrogen) heat inactivated FBS (10%) and L-glutamine (2 nM). The lipid probes used were 2-(4,4-difluoro-5, 7-dimethyl-4-bora-3a,4a-diaza-s-indacene-3-pentanoyl)-1-hexadecanoyl-*sn*-glycero-3-phospocholine (β-BODIPY FL C_5-HPC, here called BODIPY-PC), β-BODIPY FL C_5-ganglioside GM1 (here called BODIPY-GM1), or 3,3′dioctadecyloxacarbocyanine perchlorate (DiO). All lipid probes were purchased from Molecular Probes (Eugene, OR). Methyl-β-cyclodextrin (MβCD) was purchased from Sigma-Aldrich (St. Louis, MO). For imaging, 2×10^6 cells were washed in PBS and incubated with 0.5 μM BODIPY-PC or 0.5 μM BODIPY-GM1 or 0.5 μM DiO for 30 min at 4°C. After incubation, the cells were washed in cold PBS, resuspended in ~100 μM of PBS, stored on ice, and imaged between slide and coverslip at room temperature. For time-lapse measurements, cells were added to a coverslipped chamber (Nalge Nunc International, Rochester, NY), MβCD was added from stock solutions (100 mM in PBS) to a final concentration of 5 mM.

Setup

The laser illumination is provided by a mode-locked Ti:Saphire laser (Tsunami, Spectra Physics, Mountain View, CA), pumped by a 12W argon ion laser single line at 514.5 nm (Beam Lock, Spectra Physics), that produces pulses with ~100 fs full width at half-maximum (FWHM) at a repetition rate of 80 MHz and with an average power of ~1.2 W at 920 nm. The optical setup is a commercially available multi-focal multi-photon microcope (TriMScope, LaVisionBiotec GmbH, Bielefeld, Germany) connected to a modified inverted microscope (IX-71, Olympus, Tokyo, Japan) in epi-illumination geometry. A schematic of the set up can be found in Fig. 4, and a full description of a similar system in Nielsen et al. (2001). The laser illumination from the Tsunami enters the TriMScope where it passes through a waveplate/polarizer attenuator, and then a telescope to decrease the beam size. The pulse is then dispersion compensated (pre-chirp) before entering the beam multiplexer. Here the single beam is split up into two sets of 32 beams by utilizing a long 50/50 beam splitter and mirrors, one set of which has its polarization rotated by 90° with a half wave plate. These two sets of beams are recombined and passed through a 1000 Hz scanner and then illuminate and overfill the back aperture of a ×63 NA1.4 oil immersion objective (Leica Microsystems AG, Wetzlar, Germany). A line of foci is created at the focal plane, which can then be scanned across the sample and a shutter is employed to select either, both or neither of the polarizations.

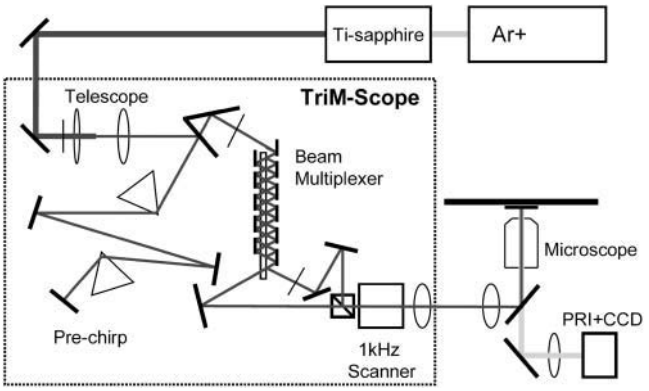

FIGURE 4 Experimental setup. Excitation is provided by an Argon ion pumped Ti:Sapphire fs laser, passed through the TriM-Scope. The IR beam is demagnified and has positive dispersion added to it to compensate for dispersion induced by the optics. The beam is then split into two sets of 32 beams by the beam multiplexer, one set of which has its polarization rotated by a half waveplate. The sets of beams are then recombined and scanned into the back aperture of the microscope. This results in a line of foci that can be scanned rapidly over the sample, and the resulting fluorescence imaged onto a polarization resolved imager (PRI) and CCD.

On the imaging side, a polarization resolved imager (Optical Insights, Tuscon, AZ) splits the image of the sample into two subimages of orthogonal polarizations using a polarizing beam splitter, one polarized parallel to the incident illumination, the other perpendicular. These two subimages are incident onto a cooled, front illumination electron multiplying CCD (Ixon, Andor Technology, Belfast, Northern Ireland). We use Imspector software developed by LaVisionBiotec to control all of the instrumentation.

LD and fluorescence anisotropy imaging

Cells were selected for imaging by looking at fluorescence in conjunction with bright-field to ensure that only healthy looking cells were studied. The focus was adjusted such that the two-photon excitation was at the equatorial region of the cell. Several frames were acquired with the EMCCD at high gain, and averaged. For time-lapse imaging, a stationary cell with circular shape was located and the LD and transmission imaged. MβCD was then added and the cells were imaged every 5–15 s with acquisition time of ~1 s for 10 min or until the cell had collapsed or moved.

Since horizontal and vertically polarized emission is simultaneously imaged on the CCD chip, these two separate subimages need to be spatially overlapped before forming the fluorescence anisotropy or LD. This is performed using home developed routines in LabView (National Instruments, Austin, TX) where the two images are translated, stretched and rotated, such that every part of the cell overlaps spatially within an error of one pixel. Thus we have images of I_{ZZ}, I_{ZY}, I_{YZ}, and I_{YY}. These then have to be corrected for several factors introduced by the instrumentation. First, for some of the data acquisition we used a polarizing beam splitter where there was 10% leakage, such that the two intensity images are not purely parallel or perpendicular. This is corrected by subtracting 10% of one image from the other (Siegel et al., 2003):

$$I_{ZZ} = 1/8(9I'_{ZZ} - I'_{ZY}) \tag{15a}$$

$$I_{ZY} = 1/8(9I'_{ZY} - I'_{ZZ}). \tag{15b}$$

Second, the imaging side of the setup could preferentially transmit one particular polarization over the other, therefore the G factor is measured to correct for this. Similarly, the excitation intensity could be greater at one polarization than the other, and therefore also an excitation factor is employed to correct for this. The G factor and excitation factor are calculated by imaging a homogenous solution of fluorescein with the same scan settings as for the cells. Thus, there are four data images for the cell: I_{ZZ}, I_{ZY}, I_{YZ}, and I_{YY}, and four images for the correction factors: C_{ZZ}, C_{ZY}, C_{YZ}, and C_{YY}. The form of the G factor (Tramier et al., 2000) and excitation factor (E) are

$$G = \sqrt{\frac{C_{ZZ}C_{YZ}}{C_{ZY}C_{YY}}} \tag{16}$$

$$E = \frac{C_{ZZ} + 2GC_{ZY}}{C_{YY} + 2GC_{YZ}}. \tag{17}$$

The steady-state fluorescence anisotropy image is formed as follows from the cell images and G factor:

$$r = \frac{I_{ZZ} - GI_{ZY}}{I_{ZZ} + 2GI_{ZY}} \tag{18}$$

The LD^r image is formed as follows from the cell images, G factor, and excitation factor:

$$LD^r = \frac{(I_{ZZ} + 2GI_{ZY}) - E(I_{YY} + 2G^{-1}I_{YZ})}{(I_{ZZ} + 2GI_{ZY}) + 2E(I_{YY} + 2G^{-1}I_{YZ})}. \tag{19}$$

These images are generated with home developed routines in MATLAB (The MathWorks, Natick, MA) and are represented as HSV images, where Hue encodes the LD^r or r value, and Value encodes the calculated isotropic absorption or emission intensity, and Saturation is at a constant maximum.

Image analysis

The cell images were analyzed with a method similar to that described earlier by Rocheleau et al. (2003). By applying a home-developed Labview routine, the LD^r is measured round the cell as a function of angle, α. An annulus is placed over the fluorescence image such that it defines the cell membrane. It is then unwrapped into a strip using bilinear interpolation. The resulting strip of LD^r values is averaged vertically (corresponding to radial direction), and binned horizontally (corresponding to tangential direction). The resulting graph of LD^r versus α is then fitted to the model described earlier, using a Gauss Newton nonlinear fitting routine, such that the mean absorption transition moment tilt with respect to the membrane normal or the LD^r modulation (LD^r at 0°–LD^r at 90°) can be derived.

Excitation polarization correction

Evaluating Eqs. 13, a–c, and 14, a and b, give significant values of M_3 and M_4 compared to M_1, with the other components contributing $<0.5\%$. This corresponds to a significant contribution from a component polarized along the optical axis (X), and absorption of this component depends on probe orientation. Experimental data were first fitted assuming perfectly polarized excitation and then corrected for the effect of the axial excitation contamination.

RESULTS

In this article, we describe a method to experimentally determine the orientation of molecules bound to membranes of living cells. To do this, images of parallel and perpendicular polarized fluorescence emission were acquired simultaneously, excited sequentially at vertical or horizontal polarization. These were then processed to form the LD^r or fluorescence anisotropy images as described in materials and methods. With the method used we assume that the calculated isotropic emission is proportional to the corresponding absorption. This assumption is not strictly accurate for an oriented sample (as discussed in supplemental information) or if the fluorophore displays different quantum yields for different photoselection (orientation). The latter has, for example, been observed with the probe Laurdan, which has emission properties sensitive to water content in the membrane. A high order of the membrane (and hence orientation of Laurdan) seem to correlate with low water content in the membrane and therefore a blue-shifted Laurdan emission (Parasassi et al., 1997). In contrast, BODIPY is very insensitive to environmental properties such as solvent polarity and pH, but can form dimeric complexes displaying weak red-shifted fluorescence (Bergström et al., 2002; Dahim et al., 2002). This has been exploited to study protein conformation (Bergström et al., 1999) or lipid trafficking within cells (Chen et al., 1997). To ensure that dimer formation was not a source of error in our measurements, the fluorescence spectrum of BODIPY-PC labeled cells was measured with a confocal microscope (TCS SP2 RS, Leica) (data not shown).

Since our method of analysis involves overlaying an annulus onto the plasma membrane, only well defined circular cells were chosen, and care was taken to image the approximate equator of the cell. We note however, that the method of analysis can be extended to analyze arbitrary shaped membrane structures. Fig. 5 shows representative images of cells labeled with the lipid probes used. These images immediately show that both the DiO and the two BODIPY probes have a degree of orientation in the cell membrane, and that they have opposite orientation to each other. The transition moment (at 920 nm) of DiO is oriented perpendicular to the lipid tails (Fig. 1) and consequently has a negative LD at $\alpha = 90°$ and $\alpha = 270°$ angles (α as defined in Fig. 2 *c*). The BODIPY probes on the other hand are inserted in the membrane and orient with the long-axis, and

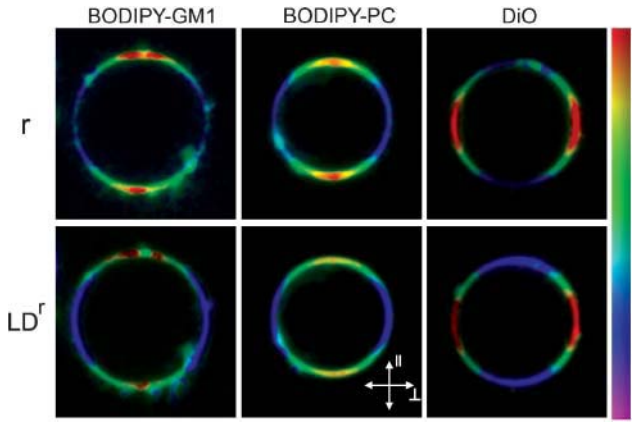

FIGURE 5 LD^r and fluorescence anisotropy (r) images. Daudi B-cells stained with BODIPY-GM1, BODIPY-PC, or DiO as indicated. DiO orients with the transition moment close to perpendicular, whereas that of the BODIPY probes is more parallel to the membrane acyl chains, giving rise to the distinct color pattern found for the different probes. The image format is HSV where Hue (*color*) represents LD^r from −0.3 to 0.3 (for BODIPY) or −0.5 to 0.5 (for DiO); and r from −0.15 to 0.6 (for BODIPY), or −0.25 to 0.6 (for DiO). Value represents calculated isotropic absorption or emission intensity, and saturation is kept constant. Parallel and perpendicular directions as indicated.

therefore the transition moment (at 920 nm) (Karolin et al., 1994), is more parallel to the lipid tails. Hence, the opposite color patterns for BODIPY and DiO. Importantly, also the steady-state anisotropy is affected by the macroscopic orientation of the probes. As a consequence, the rotational correlation times could not be estimated from the anisotropy without a model for depolarization that takes orientation into account. To experimentally isolate rotational dynamics and homo-FRET, the orientation has to be measured in conjunction with anisotropy as we do here, or alternatively time-resolved anisotropy can be imaged (Clayton et al., 2002; Suhling et al., 2004).

Evaluation of tilt angles from LD^r images

Images were analyzed by fitting the LD^r values around the cell to the derived models. This required analytically solving Eqs. 10, 12a, and 12b, and correcting the fit for high NA excitation. Although the excitation factor, E, was measured to compensate for nonuniform excitation, it did not totally compensate for the intensity differences between the two excitation polarizations, and an offset was included in the fit. Fig. 6, *A–C*, shows representative corrected experimental LD^r-values as a function of α and best fits for the three probes used, whereas Fig. 6 *D* shows the mean tilt derived from cells labeled with, BODIPY-PC ($n = 26$), BODIPY-GM1 ($n = 14$), and DiO ($n = 11$). As defined in the Theory section, perfect orientation corresponds to a tilt of 0° for all probes. Evidently, the mean of the measured tilts (49.5 ± 0.2 for BODIPY-PC, 48.0 ± 0.2 for BODIPY-GM1, and 36.2 ± 0.7 for DiO) deviate substantially from perfect orientation. However, these tilts reflect a combination of macroscopic disorder, i.e., topology of the membrane, and microscopic order dictated by lipids and other molecules in the membrane. The greater tilt of the BODIPY probes could be due to a high conformational flexibility of the chromophore inserted in the membrane. If we assume that DiO is microscopically perfectly aligned with the membrane surface and thus its only depolarizing effect comes from membrane topology we can calculate the corresponding microscopic orientation of the two BODIPY chromophores. Taking the DiO orientation of 36.2°, including high N.A. excitation effects, we work out the mean tilt of the BODIPY-GM1 to be 41° and the BODIPY-PC to be 45°. This shows that BODIPY is tilted to the general direction of the neighboring acyl chains in the membrane, most probably also tilted from intramolecular acyl chains. We note additionally that the small difference in tilt angle measured between BODIPY-PC and BODIPY-GM1 is statistically significant.

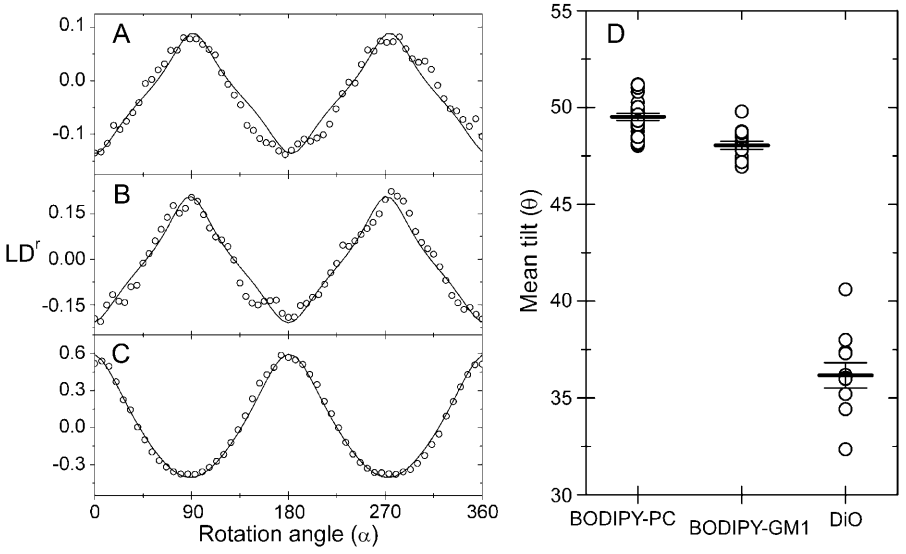

FIGURE 6 Representative plots of measured LD^r (○) as a function of angle around the cell for BODIPY-PC (*A*), BODIPY-GM1 (*B*), and DiO (*C*) stained Daudi cells. Theoretical fit for the data (*solid line*). Panel *D* shows mean tilts (*horizontal lines*) with statistical error derived from the fit for a number of cells (individual observations plotted as a *circle*). The mean tilts found were 49.5 ± 0.2° (BODIPY-PC), 48.0 ± 0.2° (BODIPY-GM1), and 36.2 ± 0.7° (DiO). Perfect orientation corresponds to 0° tilt. Measured tilt angles contain disorientation from membrane topology.

Considering distribution of orientations

In our previous analysis we have assumed the ensemble of molecules to be orientated at a fixed tilt. With such one-parameter analysis, we cannot tell the difference between a distribution of tilts or a single fixed tilt, there is just a single mean tilt. Since we are looking at a two-photon absorption process, we expect the LD^r to be a function of two parameters (Szabo, 1980) and for a two-parameter fit we can detect whether we have a single fixed tilt or a distribution of tilts. The two parameters we have in our model are $\langle\cos^2\theta\rangle$ and $\langle\cos^4\theta\rangle$, which could also be re-termed in the form of $\langle P_2\rangle$ and $\langle P_4\rangle$ order parameters. In the case of a fixed orientation $\langle\cos^2\theta\rangle^2 = \langle\cos^4\theta\rangle$, and both these two terms produce the same mean tilt angle. However, if there is a distribution of tilts $\langle\cos^2\theta\rangle^2 \neq \langle\cos^4\theta\rangle$ and the difference between the two parameters indicate the distribution of tilts. The fitted parameters $\langle\cos^2\theta\rangle$ and $\langle\cos^4\theta\rangle$ could alternatively be expressed numerically in terms of a two-parameter distribution of tilts (e.g., mean and width).

We fitted some of the data with a Gaussian distribution of tilts, but also with a sin θ term, which represents the relative space available at different tilts

$$N(\theta) = \frac{\sin\theta}{\sqrt{2\pi\sigma_\theta^2}}\exp\left(\frac{-(\theta-\mu_\theta)^2}{2\sigma_\theta^2}\right), \qquad (20)$$

where μ_θ is the mean tilt, and σ_θ is the standard deviation of the tilt distribution. Fitting for two parameters instead of one (Fig. S2, supplemental material) does give a better fit: the root mean-square error of the residuals is reduced by 20–40%. Additionally, the fitted $\langle\cos^2\theta\rangle$ and $\langle\cos^4\theta\rangle$ tilt angles differ with 95% confidence levels (data not shown), such that we can be confident that there is a distribution present. It is, however, difficult to convert these fitted values to exact mean and standard deviation tilts with accuracy we have. With our data we can resolve the distribution for the BODIPY-GM1 probe to lie somewhere between $\mu_\theta = 0°$, $\sigma_\theta = 55°$, and $\mu_\theta = 43°$, $\sigma_\theta = 22°$ with 95% confidence, which although they appear to be widely differing values, give similar-looking distributions (Fig. S3, supplemental material). For BODIPY-PC, the range is higher than for BODIPY-GM1 and generally points to a broader orientational distribution for this probe (not shown). In contrast, for DiO the range was found to be between $\mu_\theta = 0°$, $\sigma_\theta = 28°$, and $\mu_\theta = 34°$, $\sigma_\theta = 13°$ with 95% confidence, which also gives similar looking distributions and is significantly more orientated (lower mean tilt and distribution width) than for both BODIPY probes. We note, however, that assuming a single Gaussian distribution for the orientations might not describe the whole picture since earlier studies of lipid vesicles have indicated a bi-modal orientation distribution for carbocyanines (Krishna and Periasamy, 1999; Lopes and Castanho, 2004). Analysis of our DiO data considering two distributions with mean tilts fixed to 0 and 90° shows that a small perpendicularly orientated population could be present with population peak at least 3.4 times lower than that of the main population peak (Fig. S4, supplemental material). Possibly, imaging LD of these probes in giant unilamellar vesicles (GUVs) would allow greater accuracy in determining the distribution due to smaller macroscopic inhomogeneities of such vesicles.

Imaging lipid organization in membrane nanotubes

The existence of membrane nanotubes connecting cells and thereby facilitating intercellular transport of organelles and membrane was recently reported (Önfelt et al., 2004; Rustom et al., 2004). Previously, similar nanotubes have been reported to connect vesicles in constructed lipid bilayer networks (Karlsson et al., 2001). Fig. 7 shows lipid organization in membrane nanotubes between HEK 293T cells. The cells were labeled with BODIPY-PC, binding the plasma membranes and the membrane of the tube as shown schematically in Fig. 7 *B*. Fig. 7 *C* shows a stack of LD^r

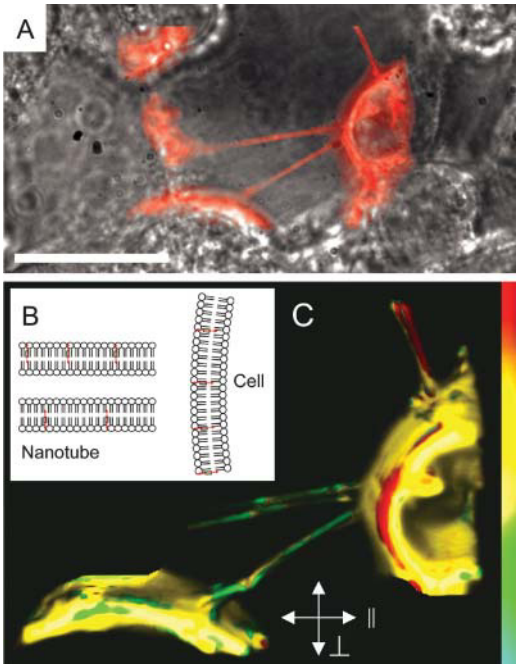

FIGURE 7 Lipid organization in membrane nanotubes. (*A*) HEK 293T cells connected by nanotubes. The small diameter of the tubes makes them invisible in the bright-field image but they are clearly visible when the BODIPY-PC fluorescence image is overlayed. The fluorescence image was acquired with a smaller sized window explaining why the tube at the top and the cells look truncated. (*B*) Schematic representation of the lipid organization in the membrane of the cell and the nanotube. The red arrow indicates the orientation of the BODIPY transition moment. (*C*) Several optical sections rendered (Volocity, Improvision Inc., Lexington, MA) to form a 3D representation of the BODIPY-PC LD^r in the two cells connected by the nanotube. The color difference between the cell and the tube reflects the opposite orientation of the membranes. Color bar represents $-0.2 < LD^r < 0.2$. Scale bar, 20 μm. Parallel and perpendicular directions as indicated.

images rendered to form a 3D representation of two of the cells and the connecting tube. The difference in color between the tube and the cell membranes corresponds to the opposite orientation of the bilayer, and hence the probe, as outlined in Fig. 7 *B*. The 3D structure was analyzed to find the mean tilt angle from the measured LD^r value. We evaluated Eqs. 12, a and b, but also accounted for the fact that the probes located at all levels in the tube are excited, not just a single plane. Analysis of the LD^r in the nanotubes (not shown) results in a tilt angle of 48.9 $\pm$1.0° compared to the 50.5 $\pm$ 0.9° found in the corresponding cell membranes.

Time-lapse imaging of cholesterol depletion

Cholesterol has been shown to be important for formation of liquid ordered domains in model membranes and is also believed to be a major constituent of lipid rafts (Simons and Ikonen, 1997; Edidin, 2003; Simons and Vaz, 2004). Cholesterol intercalates into the membrane parallel to the acyl chains, oriented with the hydroxyl group close to the hydrophilic membrane surface and the rigid tetracyclic ring structure pointing inwards. The OH group of cholesterol has been estimated to be located at roughly the same depth in the bilayer as the carbonyl oxygens in glycerophospolipids and the ring structure of cholesterol has been estimated to lie in close proximity to the first 8–10 carbons of the phospholipid acyl chains. With this mode of binding, cholesterol interacts tightly with surrounding lipids and acts to order the acyl chains, hindering isomerization around their carbon-carbon bonds (Ohvo-Rekila et al., 2002; Pandit et al., 2004). Since such interaction is also likely to effect the orientation of BODIPY inserted in the membrane we took time-lapse images of BODIPY-PC during cholesterol depletion with MβCD (Kilsdonk et al., 1995). As a control we also studied DiO that has the chromophore on the membrane surface and therefore its orientation might be predicted to be less influenced by interactions with cholesterol. Fig. 8, *A* and *B*, show LD^r images of labeled cells before ($t = 0$) and at different time points after addition of MβCD, and the corresponding LD^r values as a function of rotation angle around the cell (α) is plotted in Fig. 8, *C* and *D*, whereas panel *E* shows the LD^r modulation as a function of time. It is clearly seen that the BODIPY chromophore loses its orientation quickly: the trace for BODIPY-PC was fitted with a single exponential (red line), giving a time constant of ~26 s. For the cells studied ($n = 12$) the general trend of BODIPY losing its orientation was consistent, although the time constant varied (~15–30 s). In contrast, DiO was observed to retain its orientation for an extended period of time ($n = 7$). Even when the cell in Fig. 8 *A* (7.33 min) had collapsed by the MβCD treatment, anisotropic orientation of DiO was still evident. This shows that the rapid loss of BODIPY orientation is not due to increased macroscopic disorder (ruffling) of the membrane, since that also would affect DiO orientation. Control experiments where labeled cells were imaged under identical conditions but with no added MβCD confirmed that the loss of orientation was not caused by illumination effects such as photo-damage or local heating.

DISCUSSION

In the previous sections, we have formulated a method for measuring steady-state orientation of macroscopically orientated fluorophores by imaging two-photon linear dichroism and we have applied the method to lipid probes in cell membranes using a wide-field two-photon microscopy technique. This wide-field imaging approach provides an acceptable signal to noise with high sectioning capability at reasonably high frame rates (>1Hz) that would be difficult to achieve in a scanning microscope. Compared to wide field single photon approaches with optical sectioning (e.g., confocal microscopy using a Nipkow disk (Egner et al., 2002) or structured illumination (Neil et al., 1997)), the two-photon imaging approach offers reduced background signal and also presents some additional advantages. First, the nonlinear excitation provides two parameters describing the transition moment orientation in the cell membrane (see Results section), so that a more accurate picture of the orientation distribution can be achieved compared to one photon excitation. Second, photoselection by two-photon excitation provides stronger discrimination between weakly orientated probes, albeit with reduced discrimination for highly orientated probes. This is advantageous for this study in which the probes tend to be weakly orientated. Our studies show that, although the cell membrane is very heterogeneous and has a significant topology, we can determine the orientation of chromophores in the membrane to a useful accuracy.

Our results indicate that the surface bound probe DiO orientates with a smaller tilt angle compared to that of BODIPY-PC and BODIPY-GM1, which both have the BODIPY chromophore embedded in the membrane. The higher tilt angle found for BODIPY could be due to several factors. The chromophore could adopt a conformation where its long-axis is orientated at an angle to the intramolecular acyl chains or the orientation of BODIPY could be intrinsically low, because of high conformational flexibility, allowing a broad distribution of tilt angles. A two parameter fit to the LD^r data indicated a distribution of tilt angles, rather than fixed tilt, but the quality of the data was not high enough to accurately determine center and standard deviation of such a distribution. Previous studies of BODIPY labeled lipids have indicated that the chromophore is not perfectly aligned with the acyl chains of neighboring lipids and that this disorientation may get larger the deeper the probe is inserted into the hydrophobic region of the membrane (Johnson et al., 1991; Edmiston et al., 1996).

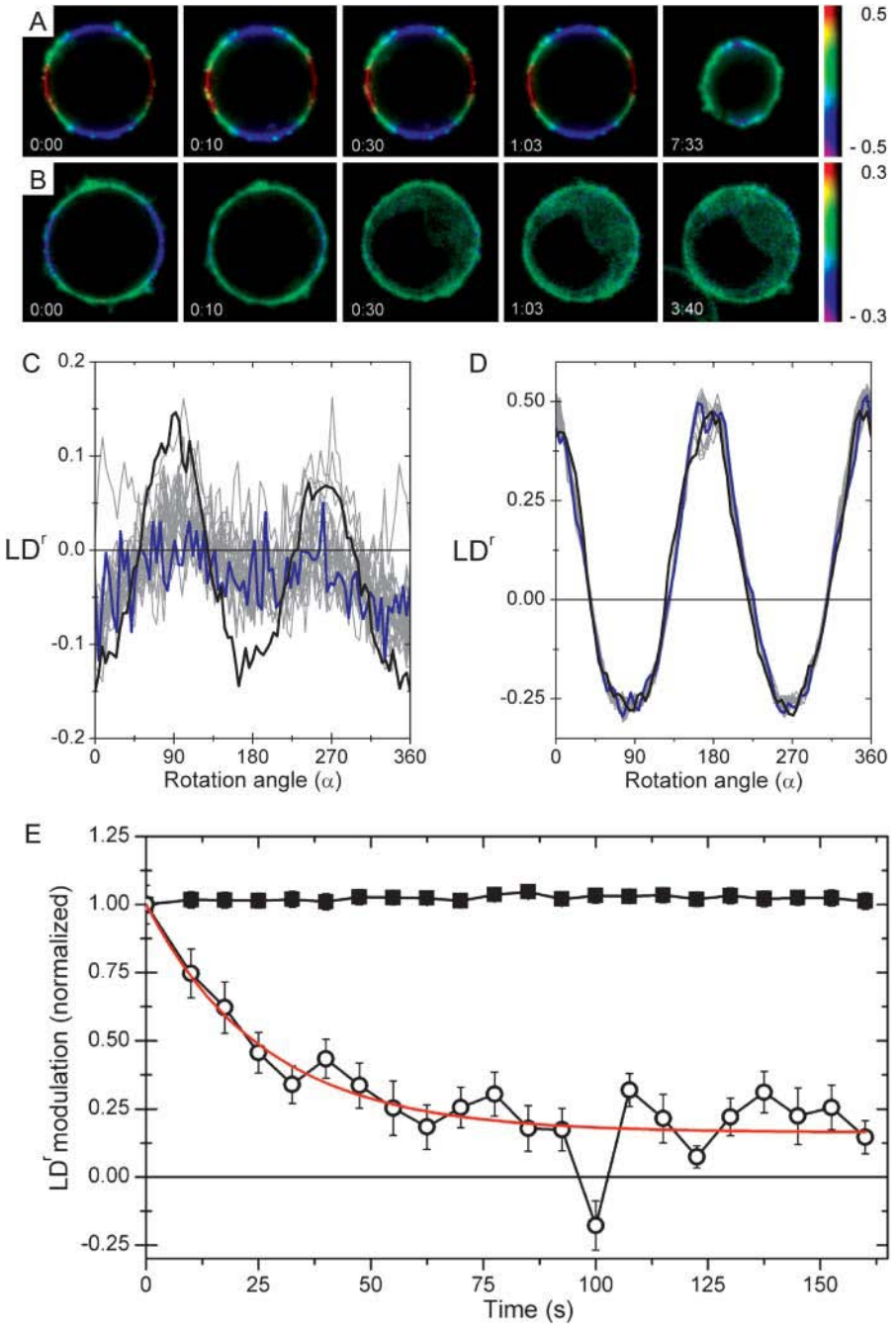

FIGURE 8 Cholesterol depletion disrupts BODIPY-PC but not DiO orientation. LD^r time-lapse imaging for representative cells stained with DiO (*A*) and BODIPY-PC (*B*) treated with MβCD (final concentration 5 mM). LD^r was imaged before addition ($t = 0$) and then every 7.5 s. The time between addition of MβCD and first image was 10 s. BODIPY-PC quickly loses its orientation, whereas DiO retains orientation for a long period of time. Panels *C* (BODIPY-PC) and *D* (DiO) show LD^r as a function of α around the cell for the individual time points where the black trace is at $t = 0$ and the blue trace is at $t = 160$ s. Panel *E* shows the normalized LD^r modulation in *C* and *D* as a function of time with 95% confidence intervals of the fits. The decay of LD^r modulation for BODIPY-PC has been fitted with a single exponential (*red line*, $y = 0.84 \exp(-t/26) + 0.16$).

The small difference in tilt angles found for BODIPY-PC and BODIPY-GM1 could be related to partition of these two probes into different domains of the plasma membrane (Edidin, 2003; Simons and Vaz, 2004). Naturally, the chemical modification by covalently attaching the BODIPY chromophore may have a significant contribution to the lipid probe's partition into domains. However, unlabeled glycosphingolipid GM1 is know to polarize to the uropod of migrating lymphocytes (Gomez-Mouton et al., 2001) and is considered to be a marker for lipid rafts (Harder et al., 1998), whereas BODIPY-PC has been reported to partition into fluid phase rather than ordered phase in lipid bilayer model systems (Korlach et al., 1999).

A consequence of working with phospholipid probes in live cells is that they can be cleaved at various positions close to the hydrophilic head groups by cellular phospholipases. Indeed, phospholipase A_2 (PLA_2) has been reported to cleave the probe BODIPY-PC at the *sn*-2 position to release a fluorescent fatty acid (Farber et al., 1999). However, the low temperature and the short incubation and imaging times used in this study should ensure low PLA_2 activity.

The orientation of BODIPY-PC in the plasma membrane is quickly lost when the cholesterol-depleting agent MβCD is added (Fig. 8). In contrast, the surface bound DiO retains its orientation during treatment with MβCD. This is evidence that cholesterol is important for packing and orientating acyl chains in the plasma membrane of cells (Ohvo-Rekila et al., 2002; Pandit et al., 2004). We note that even though the orientation of the BODIPY probes was relatively low (broad orientational distribution), it allowed us to probe the importance of cholesterol for packing and orienting the lipid tails in the membrane. An embedded probe with higher degree of orientation would give a greater dynamic range for studies of subtle processes changing the lipid environment. Also, by altering the type of lipid labeled, it may be possible to measure how the rate of cholesterol desorption depends on the interaction with different lipids (Ohvo and Slotte, 1996).

By imaging membrane nanotubes connecting cells (Fig. 7) we also demonstrate that the method may be used to study lipid organization in these small and delicate structures. Recent studies have shown that intercellular transfer of membrane and organelles can occur along such tubes (Önfelt and Davis, 2004; Önfelt et al., 2004; Rustom et al., 2004). The lipid organization in membrane nanotubes may affect transport properties of membrane molecules along the tubes or even constitute a molecular mechanism for selecting specific cell surface proteins for transport.

In the current analysis we have evaluated the orientation of the absorption transition moments of the molecules under study. By further extending the theoretical model, the anisotropy images could also be analyzed to obtain information about dynamic events such as rotational correlation and energy migration. However, it is important to note that such analysis is dependent on information (or assumptions) concerning the orientation of the studied fluorophore and its fluorescence lifetime. We note that one limitation with the current method is that it relies on the studied membrane having a well-defined shape, i.e., a perfectly round cell or a straight nanotube. A more sophisticated analysis could be implemented to account for arbitrary cell shapes. This would require local determination of the angle that the membrane makes to the laboratory axis for many points around the cell membrane, before applying the analysis presented here. This linear dichroism technique could be further extended using a differential approach. By simultaneously imaging spectrally separated probes that bind to the membrane in different locations, it may be possible to distinguish macroscopic factors, such as membrane ruffling, from factors such as changes in lipid composition.

In conclusion, the multi-focal multiphoton technique allowing wide-field detection is well-suited for high-speed 3D multi-parameter imaging such as anisotropy or linear dichroism as we have described. We also note that the method presented could be used to image molecular orientation and self-assembly (Whitesides and Grzybowski, 2002) in a range of systems not presented here. Among those could be: pathological tissue abnormalities such as amyloid fibrils (Jin et al., 2003), myosin and actin orientation during contraction or expansion of muscle fiber (Borejdo et al., 2004) or dynamic conformational analysis of individual DNA molecules.

SUPPLEMENTAL MATERIAL

An online supplement to this article can be found by visiting BJ Online at http://www.biophysj.org.
The supplemental material shows analysis of the error introduced by approximating absorption using the calculated isotropic fluorescence and fitting of LD^r images taking a distribution of tilts into account.

We are grateful to Tony Magee, Imperial College London, and Klaus Suhling, King's College London, for helpful comments on the manuscript.

This work was funded by a Beacon Award from the Department of Trade and Industry, the Medical Research Council, the Human Frontier Science Program, and the Wellcome Trust. R. K. P. Benninger acknowledges a CASE studentship supported by the Engineering and Physical Sciences Research Council and Kentech Instruments. B. Önfelt is funded by a fellowship from The Wenner-Gren Foundations.

REFERENCES

Ardhammar, M., N. Mikati, and B. Nordén. 1998. Chromophore orientation in liposome membranes probed with flow dichroism. *J. Am. Chem. Soc.* 120:9957–9958.

Axelrod, D. 1979. Carbocyanine dye orientation in red cell membrane studied by microscopic fluorescence polarization. *Biophys. J.* 26:557–574.

Bergström, F., P. Hagglöf, J. Karolin, T. Ny, and L. B. Å. Johansson. 1999. The use of site-directed fluorophore labeling and donor-donor energy migration to investigate solution structure and dynamics in proteins. *Proc. Natl. Acad. Sci. USA.* 96:12477–12481.

Bergström, F., I. Mikhalyov, P. Hagglöf, R. Wortmann, T. Ny, and L. B. Å. Johansson. 2002. Dimers of dipyrrometheneboron difluoride (BODIPY) with light spectroscopic applications in chemistry and biology. *J. Am. Chem. Soc.* 124:196–204.

Blackman, S. M., C. E. Cobb, A. H. Beth, and D. W. Piston. 1996. The orientation of eosin-5-maleimide on human erythrocyte band 3 measured by fluorescence polarization microscopy. *Biophys. J.* 71:194–208.

Borejdo, J., A. Shepard, D. Dumka, I. Akopova, J. Talent, A. Malka, and T. P. Burghardt. 2004. Changes in orientation of actin during contraction of muscle. *Biophys. J.* 86:2308–2317.

Brattwall, C. E. B., P. Lincoln, and B. Nordén. 2003. Orientation and conformation of cell-penetrating peptide penetratin in phospholipid vesicle membranes determined by polarized-light spectroscopy. *J. Am. Chem. Soc.* 125:14214–14215.

Castanho, M. A. R. B., S. Lopes, and M. Fernandes. 2003. Using UV-Vis. linear dichroism to study the orientation of molecular probes and biomolecules in lipidic membranes. *Spectroscopy.* 17:377–398.

Chen, C. S., O. C. Martin, and R. E. Pagano. 1997. Changes in the spectral properties of a plasma membrane lipid analog during the first seconds of endocytosis in living cells. *Biophys. J.* 72:37–50.

Clayton, A. H., Q. S. Hanley, D. J. Arndt-Jovin, V. Subramaniam, and T. M. Jovin. 2002. Dynamic fluorescence anisotropy imaging microscopy in the frequency domain (rFLIM). *Biophys. J.* 83:1631–1649.

Cosman, D., J. Mullberg, C. L. Sutherland, W. Chin, R. Armitage, W. Fanslow, M. Kubin, and N. J. Chalupny. 2001. ULBPs, novel MHC class

I-related molecules, bind to CMV glycoprotein UL16 and stimulate NK cytotoxicity through the NKG2D receptor. *Immunity*. 14:123–133.

Dahim, M., N. K. Mizuno, X. M. Li, W. E. Momsen, M. M. Momsen, and H. L. Brockman. 2002. Physical and photophysical characterization of a BODIPY phosphatidylcholine as a membrane probe. *Biophys. J*. 83: 1511–1524.

Davis, D. M. 2002. Assembly of the immunological synapse for T cells and NK cells. *Trends Immunol*. 23:356–363.

Dietrich, C., B. Yang, T. Fujiwara, A. Kusumi, and K. Jacobson. 2002. Relationship of lipid rafts to transient confinement zones detected by single particle tracking. *Biophys. J*. 82:274–284.

Doucey, M. A., L. Scarpellino, J. Zimmer, P. Guillaume, I. F. Luescher, C. Bron, and W. Held. 2004. Cis association of Ly49A with MHC class I restricts natural killer cell inhibition. *Nat. Immunol*. 5:328–336.

Edidin, M. 2003. The state of lipid rafts: from model membranes to cells. *Annu. Rev. Biophys. Biomol. Struct*. 32:257–283.

Edmiston, P. L., J. E. Lee, L. L. Wood, and S. S. Saavedra. 1996. Dipole orientation distributions in Langmuir-Blodgett films by planar waveguide linear dichroism and fluorescence anisotropy. *J. Phys. Chem*. 100:775–784.

Egner, A., V. Andresen, and S. W. Hell. 2002. Comparison of the axial resolution of practical Nipkow-disk confocal fluorescence microscopy with that of multifocal multiphoton microscopy: theory and experiment. *J. Microsc*. 206:24–32.

Eleme, K., S. B. Taner, B. Önfelt, L. M. Collinson, F. E. McCann, N. J. Chalupny, D. Cosman, C. Hopkins, A. I. Magee, and D. M. Davis. 2004. Cell surface organization of stress-inducible proteins ULBP and MICA that stimulate human NK cells and T cells via NKG2D. *J. Exp. Med*. 199:1005–1010.

Farber, S. A., E. S. Olson, J. D. Clark, and M. E. Halpern. 1999. Characterization of Ca2+-dependent phospholipase A2 activity during zebrafish embryogenesis. *J. Biol. Chem*. 274:19338–19346.

Gaus, K., E. Gratton, E. P. Kable, A. S. Jones, I. Gelissen, L. Kritharides, and W. Jessup. 2003. Visualizing lipid structure and raft domains in living cells with two-photon microscopy. *Proc. Natl. Acad. Sci. USA*. 100:15554–15559.

Gomez-Mouton, C., J. L. Abad, E. Mira, R. A. Lacalle, E. Gallardo, S. Jimenez-Baranda, I. Illa, A. Bernad, S. Manes, and A. C. Martinez. 2001. Segregation of leading-edge and uropod components into specific lipid rafts during T cell polarization. *Proc. Natl. Acad. Sci. USA*. 98:9642–9647.

Harder, T., P. Scheiffele, P. Verkade, and K. Simons. 1998. Lipid domain structure of the plasma membrane revealed by patching of membrane components. *J. Cell Biol*. 141:929–942.

Jin, L. W., K. A. Claborn, M. Kurimoto, M. A. Geday, I. Maezawa, F. Sohraby, M. Estrada, W. Kaminksy, and B. Kahr. 2003. Imaging linear birefringence and dichroism in cerebral amyloid pathologies. *Proc. Natl. Acad. Sci. USA*. 100:15294–15298.

Johnson, I. D., H. C. Kang, and R. P. Haugland. 1991. Fluorescent membrane probes incorporating dipyrrometheneboron difluoride fluorophores. *Anal. Biochem*. 198:228–237.

Karlsson, A., R. Karlsson, M. Karlsson, A. S. Cans, A. Strömberg, F. Ryttsen, and O. Orwar. 2001. Networks of nanotubes and containers. *Nature*. 409:150–152.

Karolin, J., L. B. Å. Johansson, L. Strandberg, and T. Ny. 1994. Fluorescence and Absorption Spectroscopic Properties of Dipyrrometheneboron Difluoride (Bodipy) Derivatives in Liquids, Lipid-Membranes, and Proteins. *J. Am. Chem. Soc*. 116:7801–7806.

Kilsdonk, E. P., P. G. Yancey, G. W. Stoudt, F. W. Bangerter, W. J. Johnson, M. C. Phillips, and G. H. Rothblat. 1995. Cellular cholesterol efflux mediated by cyclodextrins. *J. Biol. Chem*. 270:17250–17256.

Korlach, J., P. Schwille, W. W. Webb, and G. W. Feigenson. 1999. Characterization of lipid bilayer phases by confocal microscopy and fluorescence correlation spectroscopy. *Proc. Natl. Acad. Sci. USA*. 96: 8461–8466.

Krishna, M. M., and N. Periasamy. 1999. Location and orientation of DODCI in lipid bilayer membranes: effects of lipid chain length and unsaturation. *Biochim. Biophys. Acta*. 1461:58–68.

Krishna, M. M. G., and N. Periasamy. 1998. Orientational distribution of linear dye molecules in bilayer membranes. *Chem. Phys. Lett*. 298:359–367.

Kusumi, A., I. Koyama-Honda, and K. Suzuki. 2004. Molecular dynamics and interactions for creation of stimulation-induced stabilized rafts from small unstable steady-state rafts. *Traffic*. 5:213–230.

Lopes, S., and M. A. R. B. Castanho. 2004. Does aliphatic chain length influence carbocyanines' orientation in supported lipid multilayers. *J. Fluoresc*. 14:281–287.

Mitra, A. K., H. Celia, G. Ren, J. G. Luz, I. A. Wilson, and L. Teyton. 2004. Supine orientation of a murine MHC class I molecule on the membrane bilayer. *Curr. Biol*. 14:718–724.

Munro, S. 2003. Lipid rafts: elusive or illusive? *Cell*. 115:377–388.

Neil, M. A. A., R. Juškaitis, and T. Wilson. 1997. Method of obtaining-optical sectioning by using structured light in a conventional microscope. *Opt. Lett*. 22:1905–1907.

Nielsen, T., M. Frick, D. Hellweg, and P. Andresen. 2001. High efficiency beam splitter for multifocal multiphoton microscopy. *J. Microsc*. 201: 368–376.

Nordén, B., M. Kubista, and T. Kurucsev. 1992. Linear dichroism spectroscopy of nucleic acids. *Q. Rev. Biophys*. 25:51–170.

Ohvo, H., and J. P. Slotte. 1996. Cyclodextrin-mediated removal of sterols from monolayers: effects of sterol structure and phospholipids on desorption rate. *Biochemistry*. 35:8018–8024.

Ohvo-Rekila, H., B. Ramstedt, P. Leppimaki, and J. P. Slotte. 2002. Cholesterol interactions with phospholipids in membranes. *Prog. Lipid Res*. 41:66–97.

Önfelt, B., and D. M. Davis. 2004. Can membrane nanotubes facilitate communication between immune cells? *Biochem. Soc. Trans*. 32:676–678.

Önfelt, B., S. Nedvetzki, K. Yanagi, and D. M. Davis. 2004. Cutting edge: membrane nanotubes connect immune cells. *J. Immunol*. 173:1511–1513.

Pandit, S. A., D. Bostick, and M. L. Berkowitz. 2004. Complexation of phosphatidylcholine lipids with cholesterol. *Biophys. J*. 86:1345–1356.

Parasassi, T., E. Gratton, W. M. Yu, P. Wilson, and M. Levi. 1997. Two-photon fluorescence microscopy of laurdan generalized polarization domains in model and natural membranes. *Biophys. J*. 72:2413–2429.

Pralle, A., P. Keller, E. L. Florin, K. Simons, and J. K. H. Horber. 2000. Sphingolipid-cholesterol rafts diffuse as small entities in the plasma membrane of mammalian cells. *J. Cell Biol*. 148:997–1007.

Richards, B., and E. Wolf. 1959. Electromagnetic Diffraction in Optical Systems. 2. Structure of the Image Field in an Aplanatic System. *Proc. Roy. Soc. A*. 253:358–379.

Rocheleau, J. V., M. Edidin, and D. W. Piston. 2003. Intrasequence GFP in class I MHC molecules, a rigid probe for fluorescence anisotropy measurements of the membrane environment. *Biophys. J*. 84:4078–4086.

Rustom, A., R. Saffrich, I. Markovic, P. Walther, and H. H. Gerdes. 2004. Nanotubular highways for intercellular organelle transport. *Science*. 303:1007–1010.

Schuck, S., M. Honsho, K. Ekroos, A. Shevchenko, and K. Simons. 2003. Resistance of cell membranes to different detergents. *Proc. Natl. Acad. Sci. USA*. 100:5795–5800.

Siegel, J., K. Suhling, S. Lévêque-Fort, S. E. D. Webb, D. M. Davis, D. Phillips, Y. Sabharwal, and P. M. W. French. 2003. Wide-field time-resolved fluorescence anisotropy imaging (TR- FAIM): Imaging the rotational mobility of a fluorophore. *Rev. Sci. Instrum*. 74:182–192.

Simons, K., and E. Ikonen. 1997. Functional rafts in cell membranes. *Nature*. 387:569–572.

Simons, K., and W. L. Vaz. 2004. Model systems, lipid rafts, and cell membranes. *Annu. Rev. Biophys. Biomol. Struct*. 33:269–295.

Suhling, K., J. Siegel, P. M. P. Lanigan, S. Lévêque-Fort, S. E. D. Webb, D. Phillips, D. M. Davis, and P. M. W. French. 2004. Time-resolved fluorescence anisotropy imaging applied to live cells. *Opt. Lett.* 29:584–586.

Sund, S. E., J. A. Swanson, and D. Axelrod. 1999. Cell membrane orientation visualized by polarized total internal reflection fluorescence. *Biophys. J.* 77:2266–2283.

Szabo, A. 1980. Theory of polarized fluorescent emission in uniaxial liquid crystals. *J. Chem. Phys.* 72:4620–4626.

Thulstrup, E. W., and J. Michl. 1982. Orientation and linerar dichroism of symmetrical aromatic-molecules imbedded in streched polyethylene. *J. Am. Chem. Soc.* 104:5594–5604.

Toptygin, D., and L. Brand. 1993. Fluorescence decay of DPH in lipid membranes: influence of the external refractive index. *Biophys. Chem.* 48:205–220.

Tramier, M., K. Kemnitz, C. Durieux, J. Coppey, P. Denjean, R. B. Pansu, and M. Coppey-Moisan. 2000. Restrained torsional dynamics of nuclear DNA in living proliferative mammalian cells. *Biophys. J.* 78:2614–2627.

Tronin, A., J. Strzalka, X. Chen, P. L. Dutton, and J. K. Blasie. 2000. Determination of the porphyrin orientation distribution in Langmuir monolayers by polarized epifluorescence. *Langmuir.* 16:9878–9886.

Van der meer, B. W., R. P. H. Kooyman, and Y. K. Levine. 1982. A theory of fluorescence depolarization in macroscopically ordered membrane systems. *Chem. Phys.* 66:39–50.

Whitesides, G. M., and B. Grzybowski. 2002. Self-assembly at all scales. *Science.* 295:2418–2421.

Xiao, M., A. Tartakowski, O. A. Andreev, and J. Borejdo. 1996. Binding of S1(A1) and S1(A2) to F-actin. *Biochemistry.* 35:523–530.